Supplementary Information

Understanding Hierarchical Spheres-in-Grating Assembly for Bio-Inspired Colouration

Shengyang Chen,[a] Bastian Haehnle,[b] Xavier Van der Laan,[a] Alexander J.C. Kuehne,[b,c] Ioan Botiz,[d] Paul N. Stavrinou,*[e] and Natalie Stingelin,*[a,f]

[a] Department of Materials and Centre of Plastic Electronics, Imperial College London, London SW7 2AZ, United Kingdom.

[b] Institute of Organic and Macromolecular Chemistry, Ulm University, Albert-Einstein-Allee 11, 89081 Ulm, Germany.

[c] DWI – Leibniz-Institute for Interactive Materials, Forckenbeckstr. 50, 52074 Aachen, Germany.

[d] Interdisciplinary Research Institute on Bio-Nano-Sciences, Babes-Bolyai University, Treboniu Laurian nr. 42, Cluj-Napoca 400271, Romania.

[e] Department of Engineering Science, University of Oxford, Parks Road, Oxford OX1 3PJ, United Kingdom.

[f] School of Materials Science and Engineering and School of Chemical and Biochemical Engineering, Georgia Institute of Technology, Atlanta, Georgia 30332-0245, USA.

*E-mail: paul.stavrinou@lincoln.ox.ac.uk; natalie.stingelin@mse.gatech.edu

Materials

Atactic polystyrene, *a*-PS (weight-average molecular weight, $M_w \approx 192$k) and toluene (anhydrous, 99.8%) were purchased from Sigma-Aldrich. DOWSIL™ 184 silicone elastomer kit was purchased from DOW Europe. Silicon masters were purchased from NIL Technology and Phu Quy. Already-fabricated PDMS stamps were provided by Max Planck Institute for Polymer Research. Their grating parameters and schematics are summarized in Table. S1.

Table S1. Summary of gratings used in this work.

Gratings	Description	Schematics
Silicon master gratings	① Line feature, period Λ = 4 μm, width a = 2.5 μm and depth d = 2 μm; ② V-shaped feature, period Λ = 4.5 μm, apex angle ≈ 70°, depth d = 2 μm;	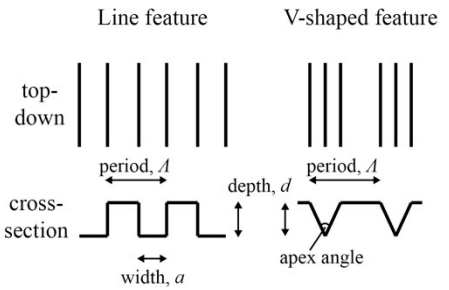
PDMS stamps (from Max Planck Institute for Polymer Research)	③ Line feature, period Λ = 4 μm, width a = 2 μm and depth d = 0.5 μm; ④ Line feature, period Λ = 1.6 μm, width a = 0.8 μm and depth d = 0.5 μm; ⑤ Line feature, period Λ = 1 μm, width a = 0.5 μm and depth d = 0.5 μm;	

Polystyrene micro-spheres of the following diameters were purchased from Sigma-Aldrich: 200 nm (10% solids), 600 nm (10% solids, std dev ≤0.03 μm), 800 nm (10% solids, std dev ≤0.03 μm), 1 μm (10% solid, std dev < 0.1 μm), and 2 μm (10% solid, std dev < 0.05 μm); while polystyrene spheres of a diameter of 0.340 μm (5% w/v, std dev ≤0.010 μm), 0.836 μm (5% w/v, std dev ≤0.024 μm), 1.28 μm (10% w/v, std dev ≤0.04 μm), 1.39 μm (10% w/v, std dev ≤0.04 μm), 2.56 μm (10% w/v, std dev ≤0.04 μm); SiO_2 particles with a diameter of 0.977 μm (5% w/v, std dev ≤0.026 μm) and polystyrene magnetic fluorescent particles of a size of 1.43 μm (10 mg/mL, std dev ≤0.07 μm) were purchased from microParticles GmbH.

Synthesis of F8DVB

F8DVB particles were synthesized via Heck-type dispersion polymerization according to a previously established protocol.[1] The monomers 2,7-diiodo-9,9-dioctyl-9H-fluorene (321.2 mg, 0.5 mmol) and divinylbenzene (65.1 mg, 71.2 μL, 0.5 mmol) and the stabilizers poly(1-vinylpyrrolidone-*co*-vinyl acetate) (7.2 g) and Triton X-45 (8 g) were dissolved in 1-propanol (66 mL, degassed) and stirred at 80 °C. Palladium(II) acetate (10.0 mg, 0.045 mmol) and tri(o-tolyl)phosphine (61.0 mg, 0.200 mmol) were dissolved in 1-propanol (10 mL, degassed) and added to the reaction mixture. The polymerization was started by adding a solution of triethylamine (210 μL, 152.5 mg) in 1-propanol (14 mL) after which it was stirred at 80 °C for 2

h under an argon blanket. For the purification, the particles were washed with a propanolic solution of Triton X-45 (1 w% in 1-propanol) three times and with pure 1-propanol four times. Each washing cycle included centrifugation (10 min, 6000 min^{-1}), decantation and redispersion of the particles.

Hot-embossing of PS films

PS gratings were fabricated via hot-embossing. First, we replicated the negative structure from the silicon master onto polydimethylsiloxane (PDMS) stamps following a previously reported protocol.[2] These PDMS stamps were cut into square shapes of a surface area of around 1 cm^2. These were then attached to the bottom of a 1 kg metal weight using double-sided tapes. Spin-coated polystyrene film on quartz or silicon substrates were subsequently transferred onto a hot plate at 170 ºC. Following that, the weight and PDMS stamps were placed on the top of the polystyrene films to emboss them for 150 s. The weight was then removed with the samples still adhered to the PDMS stamps. These architectures were cooled to room temperature where they were kept for 5 minutes before they were peeled off the PDMS stamps. The dimensions of gratings were extracted from the line profile of SEM images by averaging over 10 periods.

Self-Assembly

PS gratings were surface-treated by exposure to UV ozone for 15 minutes. A suspension (2-5% solid content) of colloidal spheres was cast onto the sample surface at room temperature. Generally, the suspension was spread by bringing the soft PDMS blade in direct contact with the sample surface, manually sweeping it back and forth along the groove direction until all water evaporated. If necessary, multiple coats were applied. In a few cases, in order to produce superstructures, a contactless hard-blade coating was used, employing a coating speed of 20 to 100 μm/s.

Optical Diffractometry

The layout of the optical diffractometer that we used is displayed in Fig. S1 (bottom). A laser beam was generated by a diode-pumped solid-state laser (473 nm) and directed through a beam chopper. The beam chopper chopped the beam into a frequency of 300 Hz, which differs from the current frequency used in England for lighting applications (50 Hz). The beam subsequently passed through a linear polarizer and a half-wave plate to alter the polarization direction prior to impinging on a beam splitter. The polarized beam was split into two beams: a small portion was led to a stationary photodiode reference detector while the majority of the beam was guided onto the sample at an angle normal to the sample surface. The grating structures in the sample diffracted the beam into a number of orders. A photodiode signal detector was programmed to move in a semi-circle trajectory to collect all transmitted, diffracted light. Detected signals from both photodiode detectors were then transferred to lock-in amplifiers, connected to the beam chopper to filter the noise signals from ambient light. For 60º and 90º cuts, samples were rotated by 60º and 90º. The polarization was set at a p-polarization with the incident electric field perpendicular to grating lines. To picture the diffraction patterns, a semi-transparent spherical half shell was used to cover the samples. The diffracted light was then projected onto the shell surface. A Canon 5D Mark ii digital camera was mounted and aligned along the optical axis. Pictures were taken in the dark to avoid the noise from ambient light. The photographs were further binarized using Adaptive thresholding via MATLAB function.

Florescence Microscopy

Fluorescence imaging was carried out using a Leica SP5 upright confocal microscope. F8DVB samples were excited at 380 nm. The detection wavelengths were set between 500 and 550 nm.

Scanning Electron Microscopy

First, a 15-nm chromium film was sputtered onto the samples to prevent them from charging. To obtain cross-sectional micrographs, the samples were immersed into liquid nitrogen for 10 s and then cleaved into two parts. The imaging was carried out using a LEO Gemini 1525 SEM with a working distance between 8 mm to 11 mm and a 5 kV accelerating voltage.

Uv-vis Spectroscopy

The samples were measured at normal incidence using a Perkin Elmer Lambda 25 Uv-vis spectrophotometer without an integrating sphere. The operating spectral range was set from 200 to 1100 nm, while the lamp changed at 326 nm. The slit width for this experiment was set at 1 nm.

Photoluminescence Spectroscopy

The emission spectra of F8DVB assembled structures were recorded via a Horiba FluoroMax 4 spectrofluorometer with an integrating sphere.

Characterisation of *a*-PS Gratings via Optical Diffractometry

The *a*-PS gratings used for the self-assembly of F8DVB spheres were characterised through Optical Diffractometry. As shown in Fig. S1 (top-panel), the diffraction profile measured has reflectional symmetry with the zero order (0º) being the axis of symmetry, which underlines the excellent homogeneity of the diffraction gratings produced. This is also indicated by the symmetric diffraction pattern displayed in the inset.

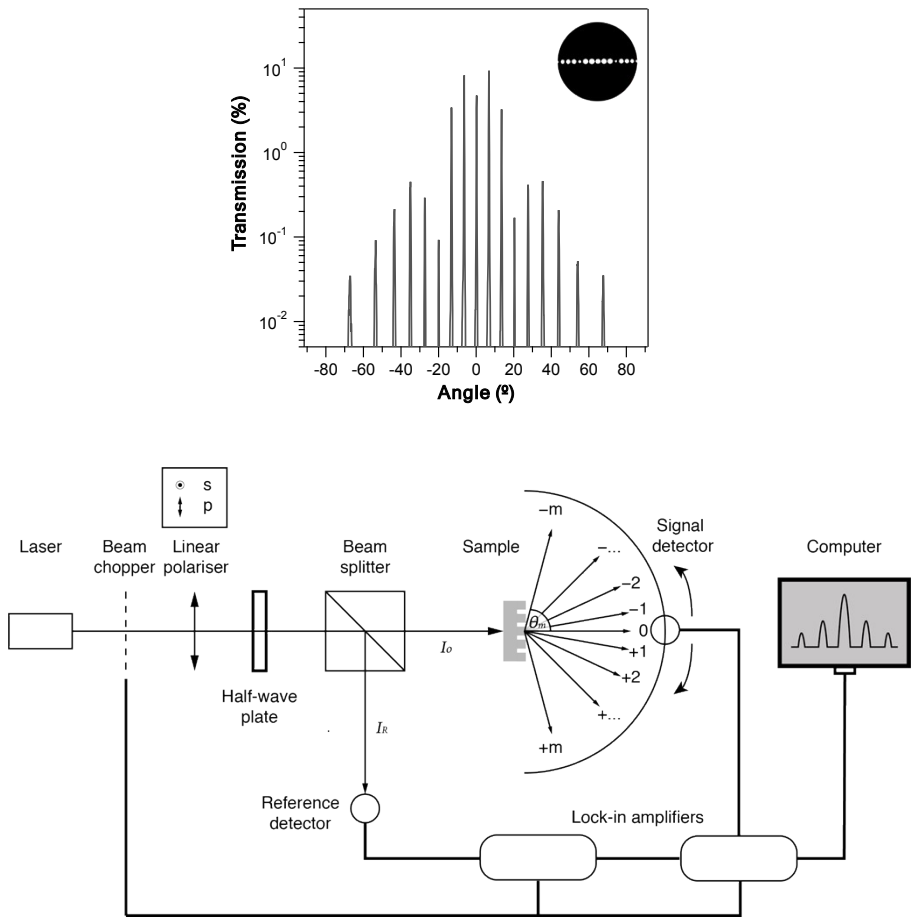

Fig. S1. Top panel: Diffraction profile of an exemplary *a*-PS grating, measured with a blue laser (473 nm, p-polarized). The diffraction pattern in the inset consists of a series of diffractions, which can be associated with the 1D nature of the grating. Bottom panel: Layout of the optical diffractometer used to measure diffraction profiles. The directions of s- and p-polarization are defined in the inset (top-left).

Spin-Coated F8DVB Thin Films: UV-Visible and Photoluminescence Spectroscopy

F8DVB spheres were dissolved in toluene and spin-coated to form a thin film on a quartz substrate. The absorption spectra of such films are displayed in Fig. S2. A broad absorption peak is found in the UV-A and blue wavelength regions. The corresponding emission spectrum obtained when using an excitation wavelength of 380 nm is also shown. The emission peak in the green wavelength window matches the fluorescence microscopy results (Fig. 1C).

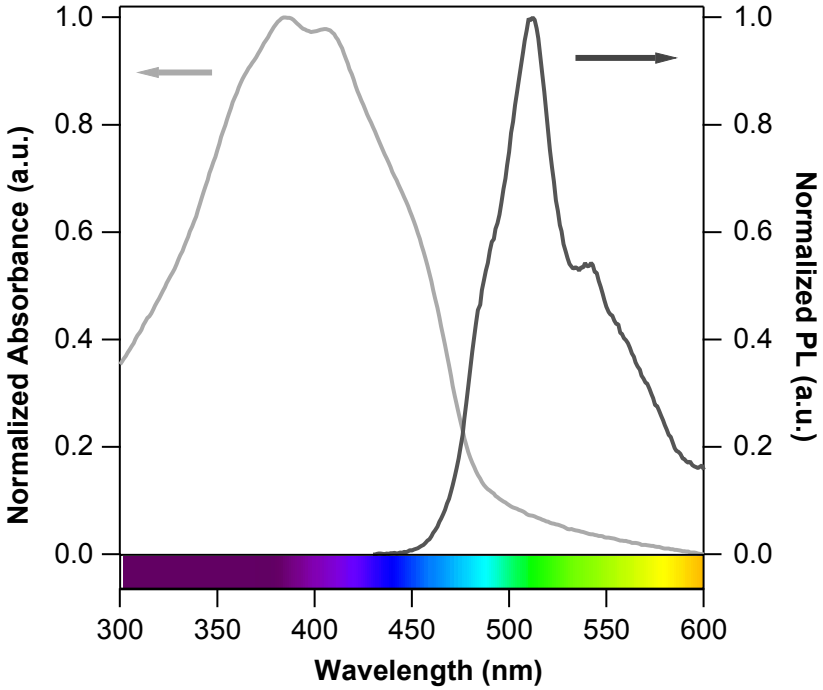

Fig. S2. UV-visible absorption and emission spectra of a F8DVB film spin-coated from a toluene solution. The F8DVB spheres were excited at 380 nm.

Fast Fourier Transforms of Gratings and Sphere Assemblies

Fourier space response of diffraction structures can be representative of their optical diffraction patterns. The origins of diffraction features were elucidated computing a Fast Fourier Transform of the diffracted structures. Column I in Fig. S3 refers to a grating-only structure, while Column II corresponds to a sphere-only (n = 2, hexagonal packing) assembly. Column III is a combination of Column I and II; Column IV is a spheres-in-grating structure with a random vertical shift of sphere arrays between two adjacent grooves as indicated in the schematic in the top row of Fig. S3. A MATLAB code was developed to construct such periodic structures for 16 grating periods (Fig. S3, row 2). FFT patterns were generated using a 'fft2' algorithm in MATLAB (Fig. S3, row 3). These Fourier transforms were then used to compare with the measured optical diffraction patterns. Reassuringly, the FFT calculation of grating-only structures is identical to the experimental diffraction pattern of the hot-embossed

polystyrene gratings shown in the inset. The periodic arrangement of spheres along the close packed directions leads to a richer diffraction as calculated by our FFT. Superimposing FFTs of different sphere assemblies with the FFT of the grating-only structure and comparing it with experimentally determined patterns for spheres-in-grating assemblies (n = 2, hexagonal packing), we can conclude that this specific sample has sphere assemblies shifted in adjacent grooves.

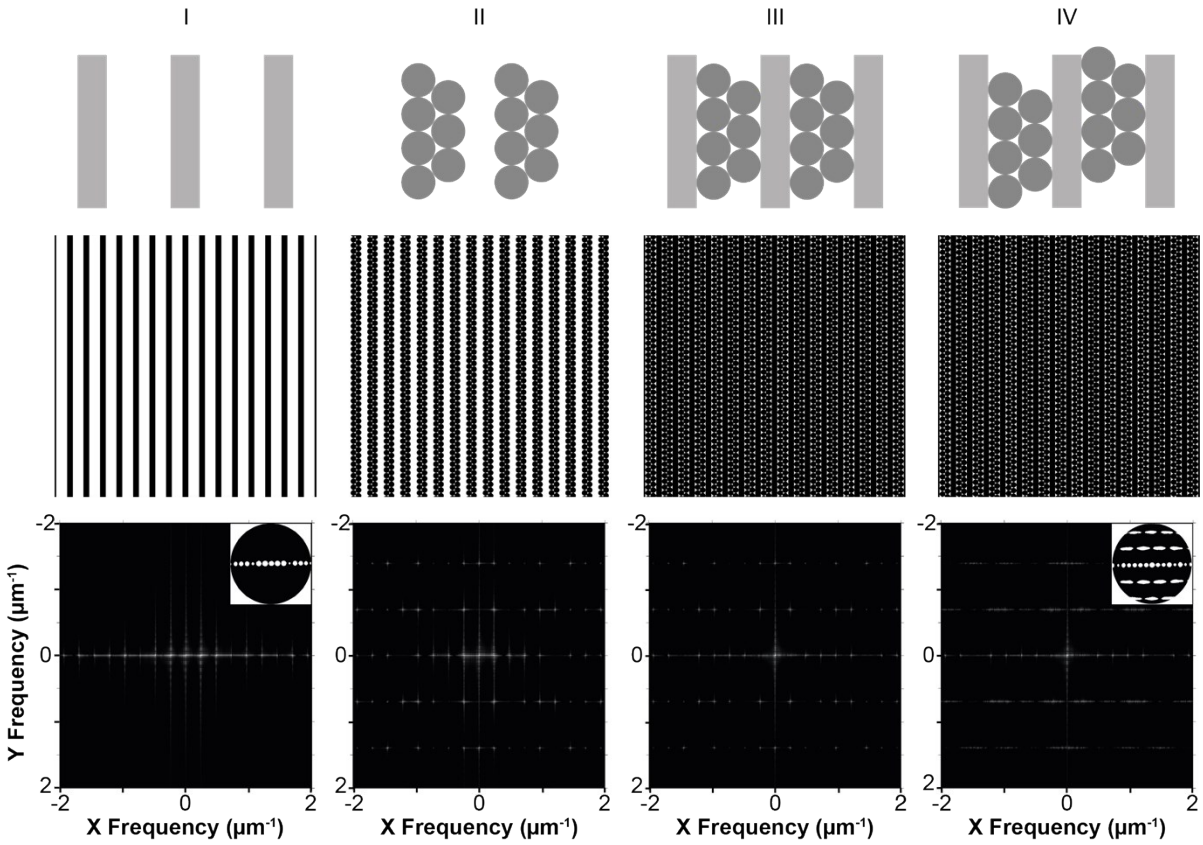

Fig. S3. Fast Fourier transforms (FFT) of calculated sphere assemblies can be used to simulate the diffraction patterns of spheres-in-grating structures. The top row shows example structures, the computed binary images of which are shown in the second row. These binary images were subsequently used for generating FFT images using a 'fft2' algorithm in MATLAB. Column I: Grating-only structure (inset: diffraction pattern of a-PS gratings, used for comparison). Column II: Hexagonally packed spheres. Column III: Spheres-in-grating structures. Column IV: Spheres-in-grating structures with a shift of sphere arrays in vertical direction in adjacent grooves similar to the one that was experimentally determined (inset).

Filling of F8DVB Spheres in *a*-PS Gratings

Additional qualitative information on the sphere arrangement and filling was obtained via contact-angle and spectral measurements. Contact-angle measurements were carried out on four samples: spin-coated polystyrene films, polystyrene gratings, spheres-in-grating structures, and drop-cast sphere monolayer (Fig. S4). The polystyrene gratings are highly hydrophobic, evident from the large contact angle of 143º. Beside the general hydrophobicity of PS, uneven surfaces as well as trapped air pockets within grooves may contribute to the high contact angle.[3] In F8DVB-spheres-in-PS-grating assemblies, the contact angle decreases to 113º. This contact angle is lower than the one measured on a F8DVB sphere monolayer (123º). Spin-coated polystyrene films displayed the lowest contact angle (96º).

For UV-vis spectroscopy, first, transmission measurements were carried out without an integrating sphere. These results provided information about the specular transmission of spheres-in-grating structures. Gratings have spatially distributed optical path lengths which change when F8DVB spheres are filled into the grating grooves. With F8DVB spheres, the difference in optical path length is significantly reduced, leading to less pronounced interference patterns. Indeed, as Fig. S4 (middle panel) shows, spheres-in-grating structures displayed the lowest transmission and the least pronounced interference oscillations compared to monolayers of spheres or PS gratings.

Finally, diffuse reflectance measurements were carried out using UV-vis spectroscopy with an integrating sphere. The results are shown in Fig. S4 (bottom panel). Since specular reflection is not included, thin-film interference effects can be discounted as the origin of any interference features observed in such samples. Polystyrene gratings were measured and oscillations were observed. In contrast to the specular transmission measurement discussed above, these oscillations are from reflected diffraction orders (apart from the zero order).[4] The sphere monolayers showed indication of resonance at wavelengths above 500 nm, possibly caused by

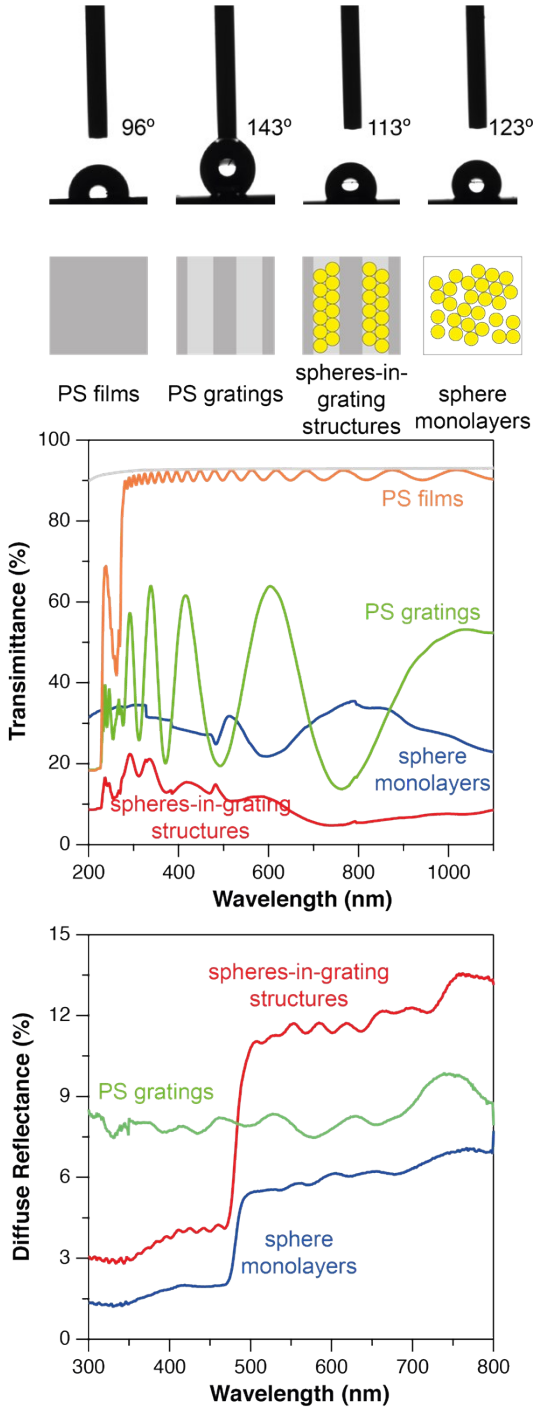

Fig. S4. Assessment of spheres-in-grating structures via contact-angle measurements and UV-vis spectroscopy. Reference PS films, PS gratings and sphere monolayers were also characterized. Top panel: Contact angles of spin-coated polystyrene films (93º), polystyrene gratings (143º), spheres-in-grating structures (113º) and drop-cast sphere monolayers (123º). The spheres-in-grating structures featured hexagonally packed spheres within grooves, while the spheres in sphere monolayers were loosely packed, leading to small domains and randomly packed features. Middle panel: UV-vis (specular) transmission spectra of these four samples measured without an integrating sphere. By assembling F8DVB spheres into polystyrene gratings, the interference oscillations from the polystyrene gratings disappeared, suggesting excellent filling. Bottom panel: UV-vis diffuse reflection spectra measured with an integrating sphere. When F8DVB spheres were introduced into the gratings, stronger scattering resonances were observed. This is probably caused by the collective diffraction from both grating and hexagonally packed spheres. In contrast, in the spectrum of sphere monolayers, the scattering resonances are not very pronounced possibly due to the poor sphere packing.

Mie scattering. These scattering resonances are vague, probably due to the irregular arrangement of the spheres in these monolayers.[5] Intriguingly, for F8DVB-spheres-in-PS-grating structures, distinct resonances are observed, which we attributed to the collective diffraction from both the ordered sphere arrays and the polystyrene grating. (Note: Light absorption of F8DVB spheres leads to the diffuse reflectance observed at around 500 nm in both sphere monolayers and spheres-in-grating structures.)

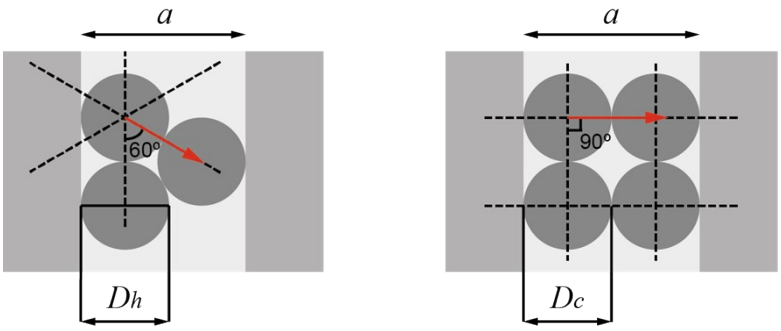

Fig. S5. Typical close-packed motifs that may form within rectangular grating grooves: hexagonal packing (left panel) and cubic packing (right panel). The red arrows represent the close packed directions and indicate the value of n (in both cases, n = 2). D_h/a and D_c/a are the optimal values for hexagonal and cubic arrays of spheres in close contact with the grating walls.

Deduction of Geometrical Relationships

Schematics of hexagonal- and cubic packing are shown in Fig. S5. The red arrows indicate the close packed directions. The number of spheres along close packed directions are noted as n. The width of gratings is a. D_h and D_c are the optimal values of sphere diameter for hexagonal and cubic packing, respectively, with spheres in close contact with grating walls. In order to achieve hexagonal packing, the below condition needs to be met:

$$\frac{1}{2}D_h + D_h \times (n-1) \times \sin 60° + \frac{1}{2}D_h = a\,. \tag{S1}$$

After simplification, we can obtain the geometrical relationship for hexagonal packing:

$$\frac{D_h}{a} = \frac{2}{2 + \sqrt{3}(n-1)}. \quad \text{(S2)}$$

Similarly, for cubic packing:

$$n \times D_c = a. \quad \text{(S3)}$$

Hence, the geometrical relationship for cubic packing can be expressed as:

$$\frac{D_c}{a} = \frac{1}{n}. \quad \text{(S4)}$$

Superstructures Formation

Superstructures formed when we used hard-blade coating and prepared samples with three different *D/a* values: 0.97, 0.58 and 0.24. Polystyrene gratings with grating depths similar to the sphere size (488 nm) were used.

A few predominant features can be found in spheres-in-grating assemblies with *D/a* 0.97 (Fig. S6). Most frequently, 1D close-packed sphere arrays (Feature 1) are observed, in agreement with the *D/a* geometrical relationship (n = 1) established in the main text. Locations where spheres assembled on top of groove walls provide insights into how multilayer spheres-in-grating assemblies are formed. For example, in Fig. S6 (Feature 2), there is one sphere assembled on two adjacent spheres in the bottom layer. Such structures are unlikely to form in an equilibrium layer-by-layer process, indicating that such structures were formed kinetically. Another example is the zig-zag configuration displayed in Fig. S6 (Feature 4). No spheres are observed on the groove bottom, suggesting that this type of assembly was not nucleated from bottom layers, unless the spheres packed as shown in Fig. S6 (Feature 1).

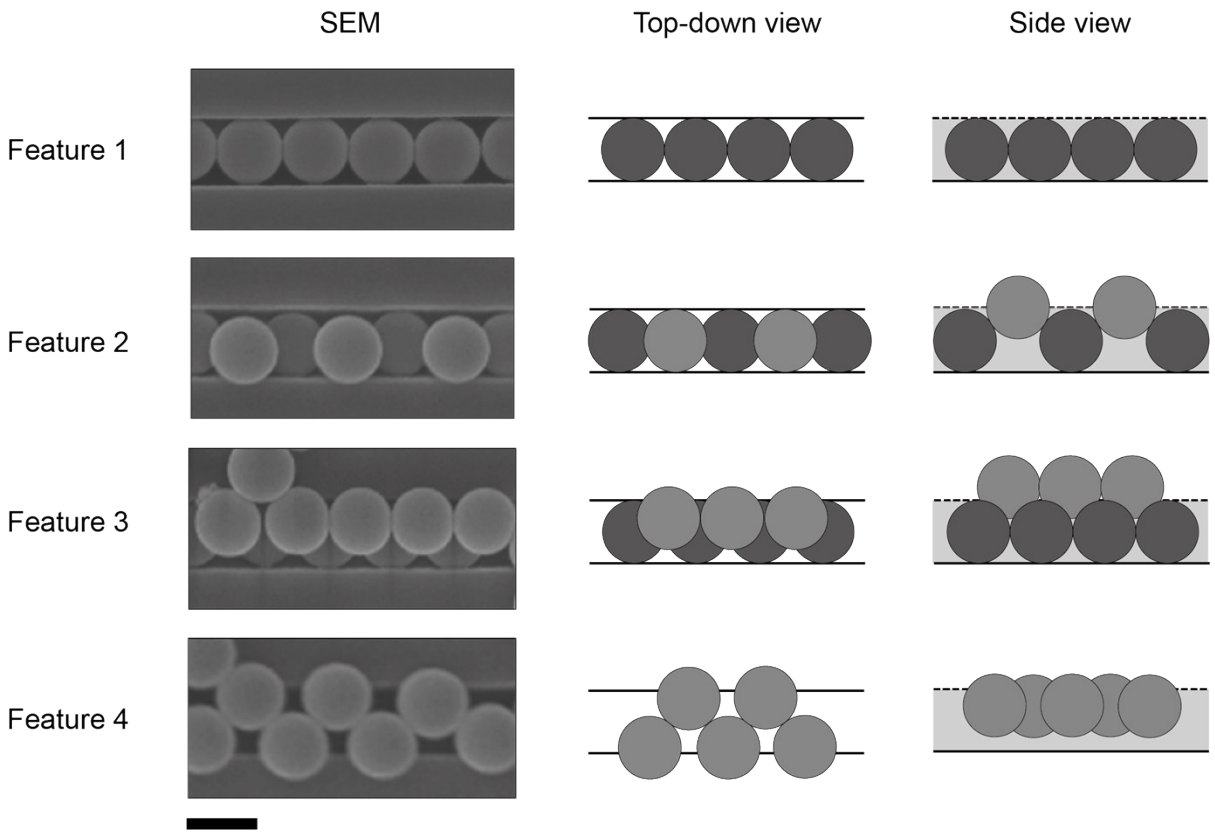

Fig. S6. Unusual spheres-in-grating assemblies in a scenario where D/a = 0.97 produced via hard-blade coating using a relatively low coating speed of 20 to 100 μm/s (T ≈ 26 ºC). Four main features can be summarized: Feature 1—Single-row assembly. Feature 2—Vertical zig-zag assembly. Feature 3—Dense, vertical zigzag assembly. Feature 4—Horizontal zig-zag assembly. Note: Feature 1 can grow into Feature 3. Feature 2 and 4 seem not to form via a layer-by-layer process. The fact that Feature 1 dominates is in agreement with the D/a geometrical relationship. Scale bar: 0.5 μm.

When D/a = 0.58, which is far from both the optimal values for hexagonal (0.54, n = 2) and cubic packing (0.50, n = 2), several interesting features can be observed (Fig. S7). In monolayer structures, horizontal zig-zags and U-shaped arrangements (Fig. S7, Feature 1 and 2) can be found, while in multilayer structures, zig-zag assemblies form horizontally and vertically (Fig. S7, Feature 3 and 4) due to the confinement effect of the groove walls. Feature 2 may further nucleate assemblies into Feature 4, while it is not entirely clear whether Feature 3 was nucleated or kinetically trapped.

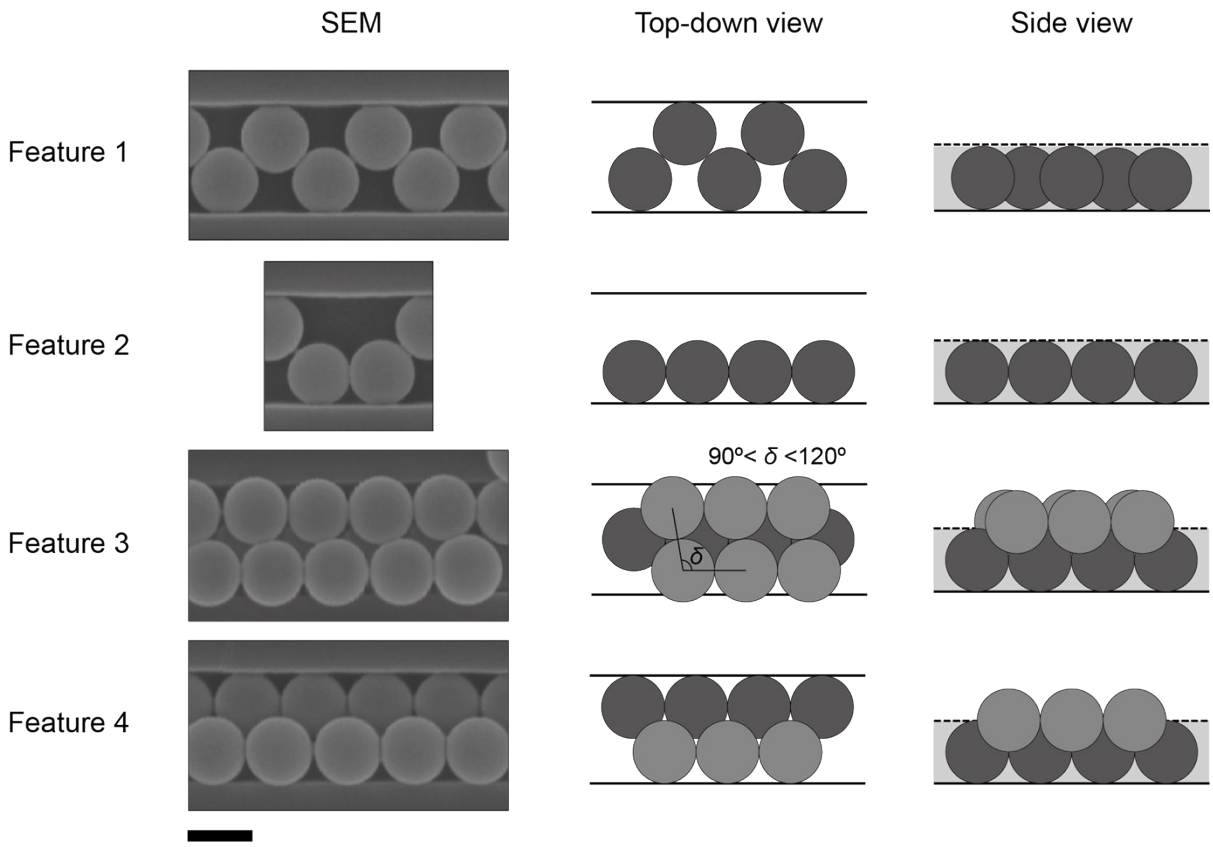

Fig. S7. Assemblies found in spheres-in-grating architectures when D/a = 0.58. Four main features were observed here: monolayer zig-zags and U-shaped structures (Feature 1 and 2), as well as bilayer zig-zags with horizontal and vertical dimensions (Feature 3 and 4). Scale bar: 0.5 μm.

As the D/a value decreases to 0.24, which is between the optimal values of hexagonal packing for n = 4 (0.28) and n = 5 (0.22), we observe a further increase in the variety of features that assemble in monolayers (Fig. F8). Energetically stable hexagonally packed domains often form, however with structural defects, leading in some cases to ordered superstructures indicated in Fig. S8 with red boxes. Randomly packed regions were also induced likely because D/a became very small (<0.22).

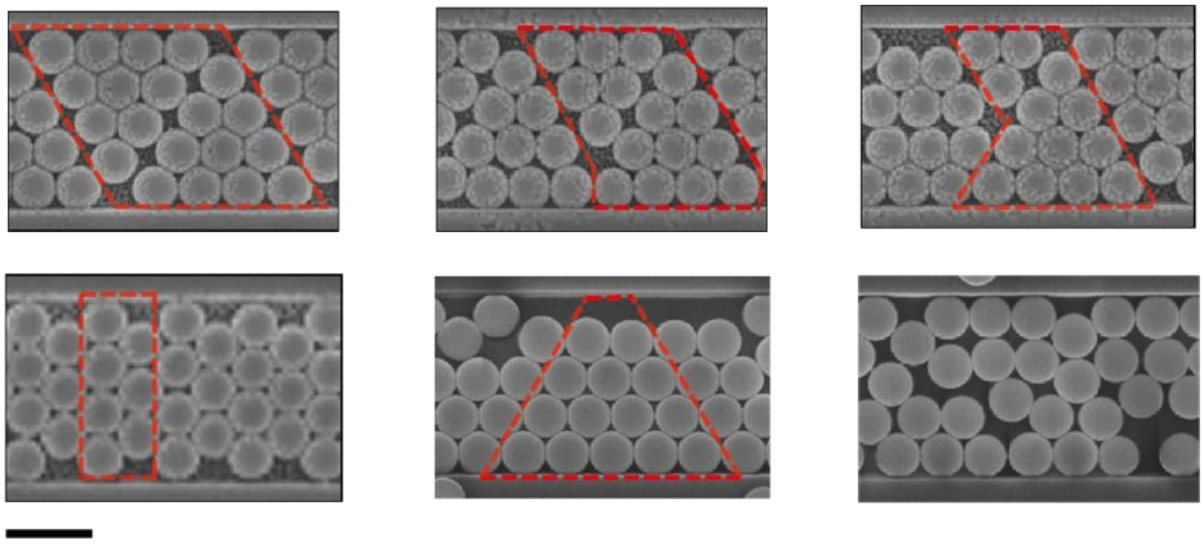

Fig. S8. Monolayer assembly of spheres-in-grating architectures when *D/a* = 0.24. Scale bar: 1 µm.

Degree of Order in Trilayer Structures

The integrated peak width, β, can be defined as:

$$\beta = {}^{DE_m}/_{T_{max_m}} \cdot M \tag{S5}$$

where ^{DE_m} refers to the absolute diffraction efficiency of the m_{th} order, $^{T_{max}}$ is the peak maximum in transmission and ^{M} is the measuring step (in radians). β can be used to obtain information on the quality of the spheres-in-grating assemblies through analysis of the peak broadness in the diffraction profiles (0º cuts, rows 5 and 6 in Fig. 3).

As shown in Fig. S9, hexagonally packed samples lead to sharper peaks in most diffraction orders compared to the ones found for randomly packed assemblies. This observation is in agreement with the fact that in hexagonally packed samples, there are fewer defects compared to those samples where random packing predominates. This often leads to scattering and broader diffraction peaks.

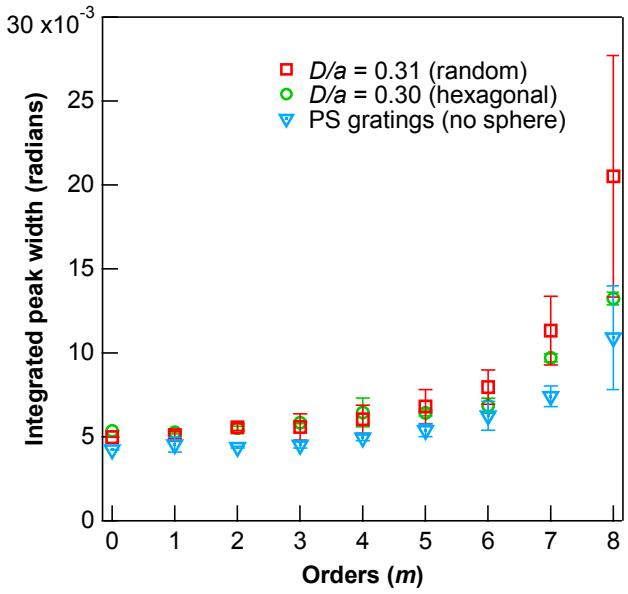

Fig. S9. In the case of trilayers, the sample with hexagonally packed spheres (D/a = 0.30) is better ordered and better filled compared to randomly packed assemblies (D/a = 0.31), in agreement with the fact that the peak widths of higher order diffractions are smaller in hexagonally packed sphere arrangements.

Adding Functions: Use of Ferroelectric Polymer Gratings

With a plethora of options to select grating- and sphere- materials, spheres-in-grating structures have tremendous potential for realising engineered architectures targeted for specific applications. A ferroelectric material exhibits an intrinsic electric polarisation, which can be altered or reversed when an external electric field is applied. Hence, ferroelectric polymer gratings may have the potential to tune/direct the assembly of charged colloidal spheres by an applied electric field.

Spheres-in-grating structures were be produced using ferroelectric poly(vinylidene fluoride-*co*-trifluoroethylene) (P(VDF-TrFE)) gratings and conjugated polymer spheres. For this, ferroelectric P(VDF-TrFE) gratings were hot-embossed across a 1 × 1 cm^2 area (Fig. S10, left panel). They displayed homogeneous light diffraction (as observed by eye), and SEM analysis underlined that the grating structures were successfully embossed (Fig. S10, middle panel). However, a significant increase in surface roughness was found compared to polystyrene

gratings, leading to wedges at the groove walls. We attribute this difference to the semicrystalline nature of P(VDF-TrFE) compared to the amorphous *a*-PS.

Colloidal spheres of the polymer emitter poly[(9,9-dioctylfuorene)-*alt*-(4,7-bis(3-hexylthien-5-yl)-2,1,3-benzothiadiazole)] (F8TBT) were assembled into such P(VDF-TrFE) gratings using again soft-blade coating, resulting in a dull, dark purple colour likely due to the formation of randomly packed spheres, as expected from the used *D/a* ratio 0.20, which is smaller than 0.22. Indeed, randomly packed spheres within grooves are observed in SEM.

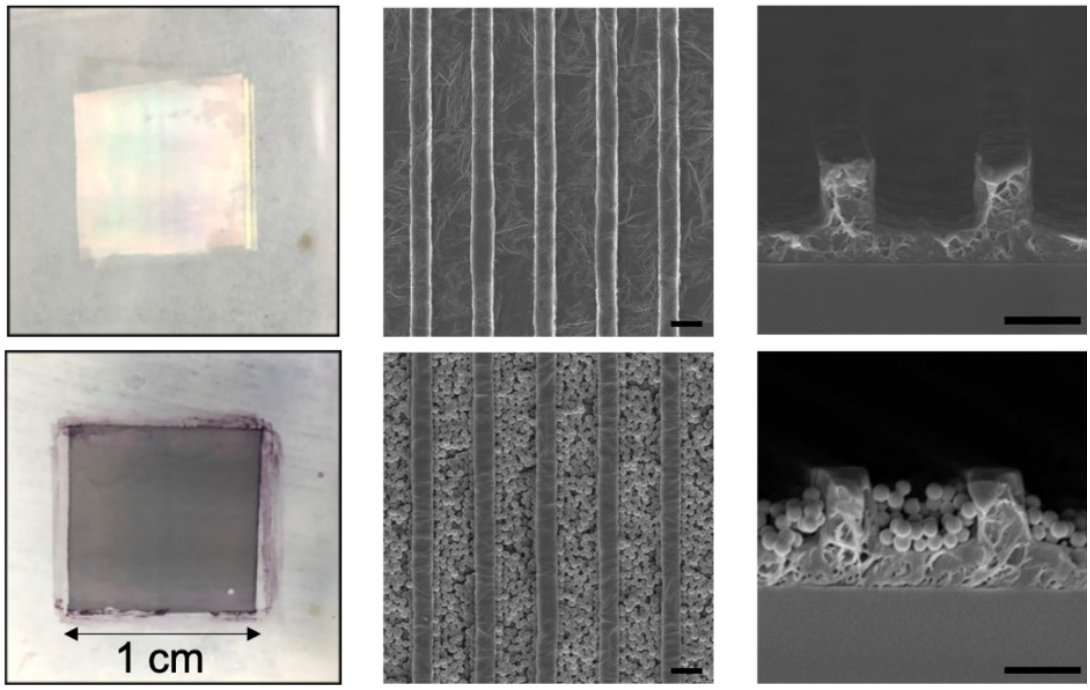

Fig. S10. Assembly of poly[(9,9-dioctylfuorene)-*alt*-(4,7-bis(3-hexylthien-5-yl)-2,1,3-benzothiadiazole)] (F8TBT) spheres into ferroelectric gratings made from poly(vinylidene fluoride-*co*-trifluoroethylene) (P(VDF-TrFE)). Left panel: Photographs of P(VDF-TrFE) gratings and F8TBT-spheres-in-grating structures. Patterned areas are 1 × 1 cm^2. Middle and right panels: SEM top-down and cross-sectional micrographs. Scale bars: 2 µm. As expected from the *D/a* value 0.20, which is below 0.22, randomly packed spheres are observed in SEM (bottom-middle panel).

References

1 S. Ciftci and A. J. C. Kuehne, *Macromolecules*, 2015, **48**, 8389–8393.

2 D. Qin, Y. Xia and G. M. Whitesides, *Nat. Protoc.*, 2010, **5**, 491–502.

3 B. Bhushan, *Biomimetics: bioinspired hierarchical-structured surfaces for green science and technology*, Springer, 2016.

4 T. Aho, M. Guina, F. Elsehrawy, F. Cappelluti, M. Raappana, A. Tukiainen, A. B. M. K. Alam, I. Vartiainen, M. Kuittinen and T. Niemi, *Opt. Express*, 2018, **26**, A331–A340.

5 P. Sheng, *Scattering and localization of classical waves in random media*, World Scientific, London, 1990.